https://doi.org/10.2352/EI.2023.35.6.ISS-344

Reset Noise Reduction Method in 3-T Pixels

Kaitlin M. Anagnost, Xin Yue, Eric R. Fossum; Dartmouth College; Hanover, NH/USA

Abstract

A reset noise reduction method using a feedback amplifier that results in an 80% noise reduction in 3-transistor (3-T) pixels is presented. 3-T pixels are useful for non-visible imaging applications because they have fewer post-processing issues than 4-T pixels and do not require charge transfer. They suffer from reset noise because correlated-double sampling cannot be realized without additional memory. Analysis of the experimental power spectral density indicates potential for further noise cancellation in future devices.

Introduction

Imaging outside the visible spectral regime is frequently achieved by depositing a foreign material on the silicon sensing layer to improve quantum efficiency. Silicon-based infrared (IR) detectors, for example, use this technique for astronomy, surgical, light detection and ranging (LiDAR) applications, and more. Indirect x-ray detectors also use a scintillating material to achieve an enhanced wavelength response for medical, scientific, industrial, and other applications.

4-T pixels present post-processing challenges including containing many dielectric layers and contacts, thus etching can result in a higher chance of causing defects and damaging the sample. During the etching and deposition process in a 4-T pixel, first a mask is made to prevent the material from being deposited on the in-pixel transistors. The transfer gate (TG) may be in a problematic location and may not be protected from the mask, exposing it to the etching and deposition process. The interlayer and intermetal dielectrics are then etched down in the regions without the mask before the foreign material is deposited. If they are not etched away completely, the dielectrics insulate the TG from the conductive exotic material. The TG then cannot be biased high enough to transfer the charge from the photodiode (PD) to the floating diffusion. To avoid this problem, many non-visible detectors neglect the TG completely.

CMOS image sensor pixels without a TG and containing only a row select, reset, and source follower (SF) transistor may be used instead, as shown in Figure 1a. Known as a 3-T pixel, it undergoes the integration period first and is reset after, as depicted in Figure 1b. The lack of a TG results in two major changes compared to the typical 4-T pixel: 1) There is only a single storage element in the pixel and 2) True correlated double sampling (CDS) cannot be implemented [1]. Without two storage elements, the pixel has more space for a single, large photodiode, which is useful for applications such as x-ray imaging. Larger photodiodes are more suitable for 3-T pixels because no charge transfer is necessary. Complete and expedient charge transfer is notoriously difficult in 4-T pixels and is avoided altogether in 3-T pixels via nondestructive readout with the PD alone. Additionally, 3-T pixels are easier to fabricate than 4-T pixels and therefore cheaper. The post-processing issues involving 4-T pixels are also less onerous with 3-T pixels.

Without a second storage node, however, CDS cannot be easily performed, resulting in higher reset noise. The pixel does not have correlated noise between its output and reset signals within the same frame because the reset occurs after the signal is readout. The reset cannot readily take place before the integration period in the same frame as in a 4-T pixel because the signal would be lost. As a result, the noise from the reset period in frame n-1 correlates to the noise in the photo signal in frame n. If these signals were stored in sampling capacitors as in 4-T chips, leakage would degrade the signal integrity due to the long storage period. The noise reduction would then be diminished compared to the 4-T case when the signals are subtracted. While analog CDS cannot be easily implemented, the output and reset signals can be stored and subtracted in the digital domain, but at the cost of more space [2]. Consequently, a technique to reduce the reset noise in 3-T pixels is needed.

Method

As shown in the schematic in Figure 2a, a column feedback amplifier (CFBA) is connected to the reset gate. Not shown are two pass gates to separate the amplifier's output from the reset gate and ground the reset gate when it is not in use. The amplifier's positive input is connected to a ramp generator that decreases during the reset period, as illustrated in the timing diagram in Figure 2b. Initially, the common mode voltage of the amplifier is too high, causing it to rail. As the positive input decreases, the common mode voltage lowers, and the amplifier's output decreases until the end of the reset period.

Several papers ([1], [3], [4]) propose using CFBAs to cancel noise at the PD to reduce reset noise in 3-T pixels. [1] and [3] connect the amplifier's output to the reset drain – a low impedance node. As a result, both papers utilize a SF buffer at the amplifier's output, increasing the area, power, and complexity. [4] instead connects the amplifier's output to the reset transistor's gate and ramps the amplifier's reference voltage up. One may expect the reset noise to get worse because the transistor will turn off more abruptly, but [4] reports reduced noise. The authors of this paper simulated this method and found the noise increased. To reduce reset noise without these challenges, the technique presented here connects the CFBA to the reset gate while ramping the amplifier's reference voltage down to turn off the reset transistor softly.

This method obtains bidirectional current at the PD to cancel reset noise using the CFBA. For example, when the PD experiences a positive change in current due to noise, this perturbation is reflected at the CFBA's negative input. It correspondingly produces a voltage 180 degrees out of phase with this disturbance and the reset gate is modulated with a negative voltage fluctuation. This voltage change causes the NMOS reset transistor to turn off more, creating a negative shift in current at the PD and cancelling the noise with bidirectional current.

The noise spectrum of interest must first be identified to understand the system. The two primary noise contributions are flicker and kTC noise caused by the in-pixel SF and reset transistor, respectively. A theoretical frequency response curve of the system is illustrated in Figure 3a, with the characteristic 1/f noise tail shown at the low frequency end of the spectrum. Since kTC noise is white, its contribution is illustrated by the flat portion

of the plot. The reset transistor's channel resistance and PD's capacitance are modeled as a low-pass filter (LPF) in Figure 3b. The pixel's low-pass filtering behavior causes the response to roll off at the bandwidth of the system, determined by its RC time constant. Therefore, the primary noise of interest is the amplitude of the LPF's frequency response, or the kTC noise contribution.

Results

This method was designed and fabricated using a 180 nm process to obtain proof-of-concept using a single pixel due to time limitations and foundry availability. The reset noise test was run by pulsing the reset gate using the CFBA and sampling the chip's output once per period, repeated 2.5 million times. The resulting power spectral density (PSD) of the sampled voltage is plotted and shown in Figure 4a, with the forward and backward sum of the data in Figure 4b and 4c, respectively. The standard deviation of the samples is 160 μV rms, or read noise 12 e- rms, resulting in ~80% noise reduction from a control pixel. The PSD of a LPF with a 24 Hz corner frequency and 25 $\mu V/\sqrt{Hz}$ amplitude is overlayed on the PSD of the data in Figure 4a and matches well, validating the model.

The forward and backward sum elucidate the noise contributions at different frequencies. Both curves are smooth, indicating the noise is white, as expected, and none of the harmonics shown in the PSD have significant energy. The forward sum illustrates that much of the noise contribution is from 5 – 100 Hz. Some applications may be concerned with noise closer to the sampling frequency, and may choose to neglect these contributions, for example. The backward sum plot shows the low frequency noise (<5 Hz) has minimal contributions and also may be discounted in applications concerned with high-frequency noise.

The reset noise test was repeated with varying reset pulse widths, with the resulting PSDs plotted in Figure 5a and corresponding noise in Figure 5b. As the reset time increased, the amplitude of the PSD decreased, and corner frequency increased. The amplitude and noise were lower with longer reset times because the CFBA had more time to operate in the high gain, noise cancellation region. The corner frequency shift was a consequence of the decrease in amplitude; the frequency response curve was shifted down, causing the corner frequency to increase. As illustrated in Figure 5b, longer reset times resulted in less noise. More effective noise cancellation results in lower amplitude PSDs with higher corner frequencies as the frequency response curve is lowered.

To eliminate more reset noise, correlated multiple sampling (CMS) was performed on the data post-processing, as shown in Figure 6. The inverse of the square root of the number of CMS samples N, or $1/\sqrt{N}$, was also plotted and is nearly identical to the CMS data, proving the samples are independent. With 32 CMS samples, for example, the noise is reduced to less than 30 μV rms, or 3 e- rms.

Conclusions and Future Work

To improve the technique, the simulation model files were first adjusted to match the lab data using the original amplifier. The amplifier was then substituted with an ideal, single-pole amplifier. The reset noise test was performed using Virtuoso's pss and pnoise simulations in which the harmonics of the system are calculated over a specified frequency range.

The PSD of a simulation using an ideal op amp with 100 gain and 1 MHz unity gain frequency (UGF) with varying reset pulse widths is presented in Figure 7a. As illustrated, the amplitudes of the PSDs decrease with longer reset times while the corner frequencies increase, matching the experimental data's trend. The corner frequencies are higher than expected due to an inaccuracy in modeling the reset transistor's off-resistance and does not affect the accuracy of the PSD's amplitude. The corresponding transient result is shown in Figure 7b. Initially, the common mode voltage of the op amp is too high, causing it to rail. As its reference voltage decreases, however, the common mode voltage lowers sufficiently to track the pixel's output and cancel noise. The resulting signal levels, noise, and signal to noise ratios (SNRs) for this simulation are displayed in Table 1. The signal is defined as the pixel's output during the reset period and as expected, increases with longer reset times. The noise was calculated by taking the maximum of the forward and backward sums. It generally decreases with longer reset times but is much higher than the experimental data due to the incorrect corner frequency. Correspondingly, the SNR increases with larger reset times.

The above baseline simulation was altered to find the limits of the noise cancellation technique. Since a shorter reset time is desired, the simulation was repeated using a 5 μsec reset time while maintaining the ideal amplifier's gain bandwidth product (GBP). Figure 8a and 8b show the resulting PSD and transient result, respectively, while Table 2 displays the signal, noise, and SNR. Figure 8a illustrates that increasing the gain while decreasing the amplifier's bandwidth lowers the PSD's amplitude, reducing the noise. However, as depicted in Figure 8b, the amplifier's lower UGF causes the pixel to be reset slower, resulting in a smaller signal. For the slowest op amp, the PD will not initially be reset to VDD-Vth in the given reset period and may increase image lag. Nevertheless, the 200 gain, 500 kHz UGF case results in the best SNR, as indicated in Table 2. The 100 gain, 1 MHz op amp yields lower noise than the long reset simulations illustrated in Figure 7a. This result may be due to the signal itself getting filtered as well as the lower duty cycle associated with a smaller reset period. Low frequency harmonics in lower duty cycle signals typically have smaller amplitudes than in large duty cycle signals. Since the system acts like a low-pass filter, these harmonics remain and are attenuated further by the CFBA, resulting in less noise.

The technique presented here currently reduces the reset noise in 3-T pixels by ~80% by utilizing a CFBA, but subsequent analysis shows the possibility of enhanced noise reduction. Performing CMS can reduce the noise further by $1/\sqrt{N}$, for example. The PSDs of the experimental data also give insight into how the technique operates and help form predictions for future designs. For example, increasing the amplifier's gain and decreasing its UGF will reduce the noise. Overall, the current design shows promise for reducing the noise in future iterations.

References

[1] N. Teranishi, "Analysis of Subthreshold Current Reset Noise in Image Sensors," *Sensors*, vol. 16, no. 5, Art. no. 5, May 2016, doi: 10.3390/s16050663.

[2] T. Watabe, Y. Honda, M. Nanba, H. Ohtake, and M. Kubota, "Three-transistor-pixel CMOS image sensor for 8K Super Hi-Vision stacked sensor with highly sensitive photoconversion layer," presented at the

2017 International Image Sensor Workshop, Hiroshima, Japan, p. 4. [Online]. Available: https://www.imagesensors.org/Past%20Workshops/2017%20Workshop/2017%20Papers/P44.pdf

[3] M. Ishii *et al.*, "An ultra-low noise photoconductive film image sensor with a high-speed column feedback amplifier noise canceller," presented at the 2013 Symposium on VLSI Circuits, pp. C8–C9. [Online]. Available: https://ieeexplore.ieee.org/document/6578706

[4] B. Pain, T. J. Cunningham, B. Hancock, G. Yang, S. Seshadri, and M. Ortiz, "Reset noise suppression in two-dimensional CMOS photodiode pixels through column-based feedback-reset," in *Digest. International Electron Devices Meeting,* Dec. 2002, pp. 809–812. doi: 10.1109/IEDM.2002.1175961.

Acknowledgements

The author would like to thank Bob Barry, Kishalay Datta, and Yanqiao Li for their enlightening discussions.

Author Biography

Kaitlin Anagnost received her BS in physics from the University of California, San Diego (2018) and is currently pursuing her PhD in engineering sciences from Dartmouth College. Her work has focused on extending the wavelength response of photon-counting image sensors.

Xin Yue received his Bachelor of Science from the Wuhan University of Technology (2011) and his Master of Science from the University of Southern California (2013). He was employed as a mixed signal circuit design engineer at Forza Silicon, CA for 7 years. Currently, he is pursuing his Ph.D. in engineering sciences from Dartmouth College. His work predominantly focuses on ultra-high speed, low noise, advanced image sensor design.

Eric R. Fossum is the John H. Krehbiel Sr. Professor for Emerging Technologies with the Thayer School of Engineering, Dartmouth College. He is the primary inventor of the CMOS image sensor used in billions of smartphones and other applications and is currently exploring the quanta image sensor. He was awarded the IEEE Andrew Grove Award, the Queen Elizabeth Prize for Engineering in 2017, the OSA/IS&T Land Medal in 2020, and the Technical Emmy Award in 2021, among other honors. He was the Co-Founder and the First President of the International Image Sensor Society. He was inducted into the National Inventors Hall of Fame and is a Member of the National Academy of Engineering.

Figures

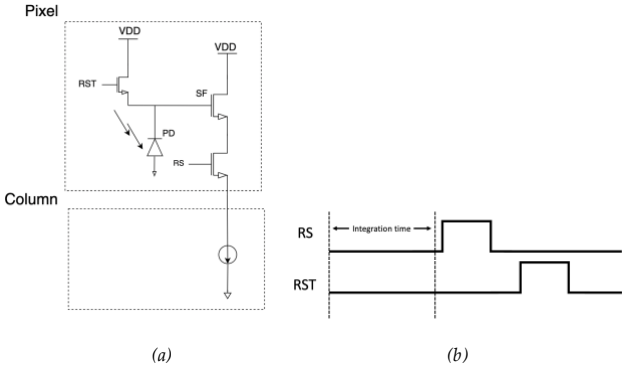

Figure 1. (a) Schematic representation of 3T pixel with RST, SF, and RS transistors. (b) Associated timing diagram.

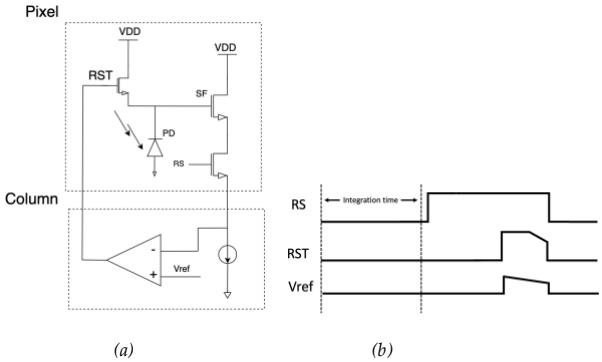

Figure 2. (a) Simplified schematic of proposed feedback reset method and (b) timing diagram.

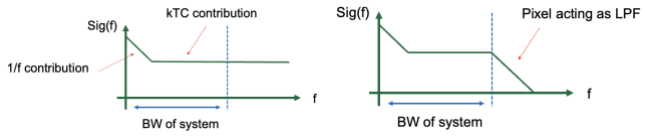

Figure 3. Theoretical frequency response of system (a) without and (b) with the pixel.

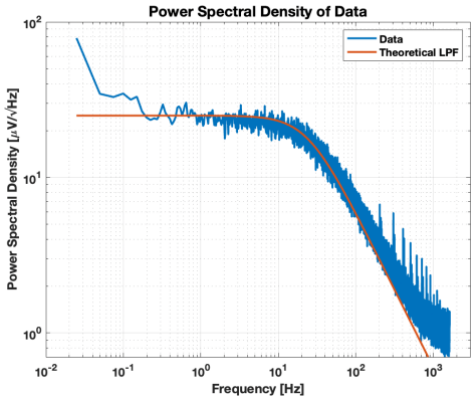

(a)

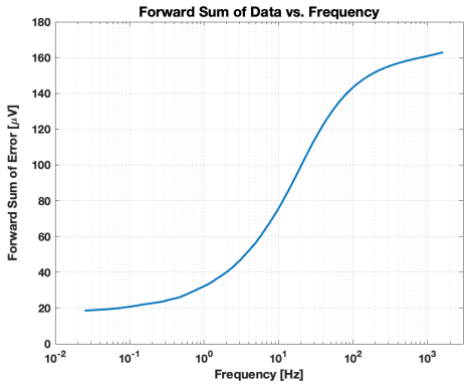

(b)

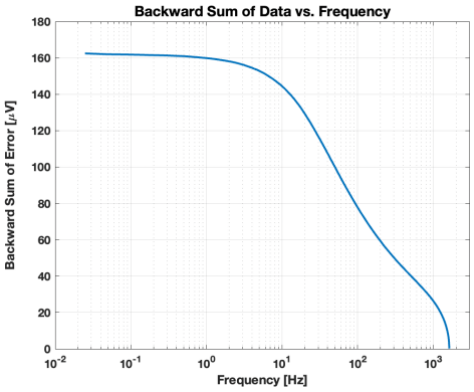

(c)

Figure 4. (a) Reset noise test PSD. (b) Forward sum and (c) backward sum of data vs. frequency.

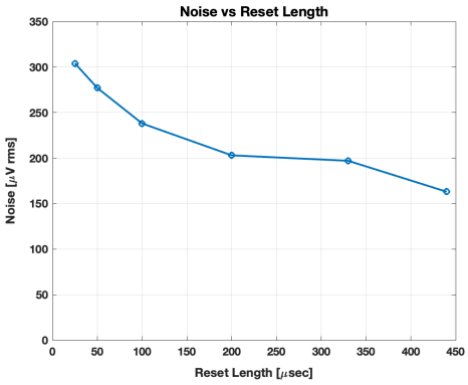

(b)

Figure 5. (a) PSDs for reset noise tests with varying reset times. (b) Resulting noise vs reset length.

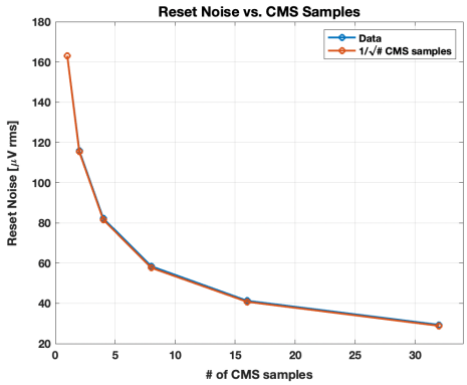

Figure 6. Reset noise vs. CMS samples using the 160 μV rms result.

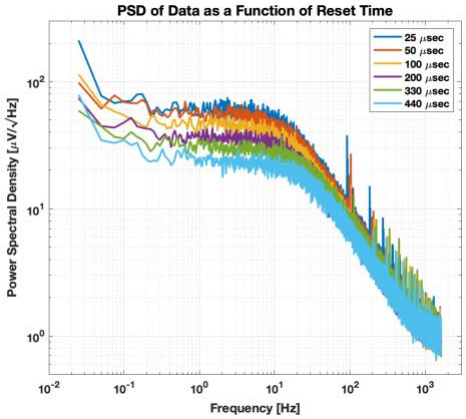

(a)

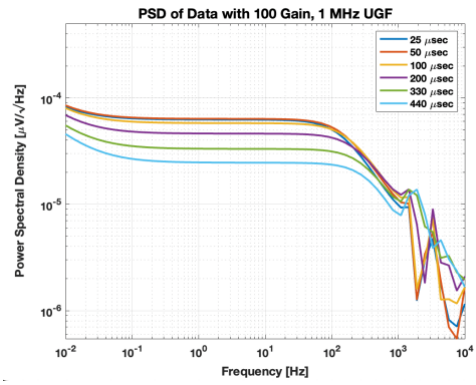

(a)

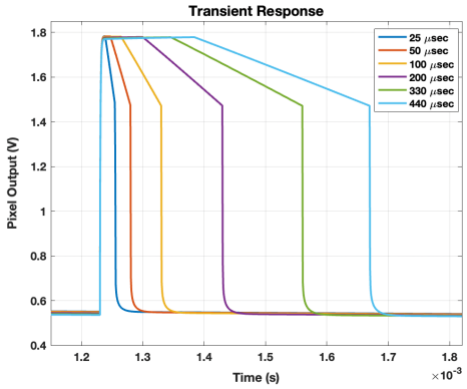

(b)

Figure 7. (a) PSDs for baseline simulation reset noise tests with varying reset times. (b) Transient result.

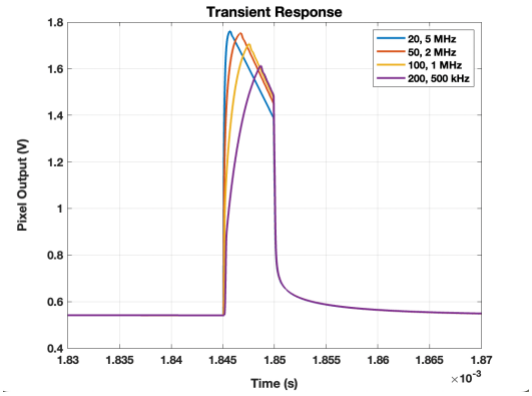

(b)

Figure 8. (a) PSDs for reset noise tests with 5 μsec reset time. (b) Transient result.

Table 1: Signal, Noise, and SNR of Baseline Simulation

Reset time	Signal (V rms)	Noise (mV rms)	SNR
25 μsec	1.53	4.2	51
50 μsec	1.54	4.3	51
100 μsec	1.61	4.1	52
200 μsec	1.64	3.7	53
330 μsec	1.66	3.3	54
440 μsec	1.66	2.9	55

Table 2: Signal, Noise, and SNR of 5 μsec Simulation

Amp gain, UGF	Signal (V rms)	Noise (mV rms)	SNR
20, 5 MHz	1.47	3.7	52
50, 2 MHz	1.49	3.4	53
100, 1 MHz	1.43	2.5	55
200, 500 kHz	1.30	0.99	62

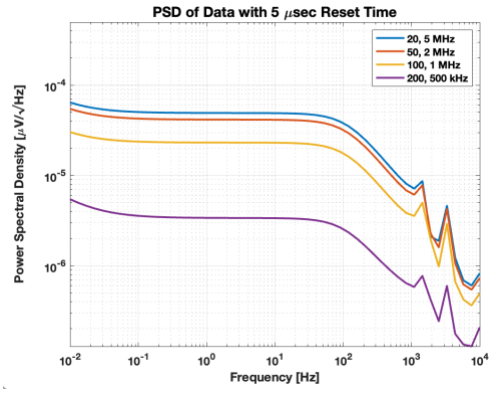

(a)